Radiology

ORIGINAL RESEARCH • VASCULAR AND INTERVENTIONAL RADIOLOGY

Ablative Margins of Colorectal Liver Metastases Using Deformable CT Image Registration and Autosegmentation

Yuan-Mao Lin, MD • Iwan Paolucci, PhD • Caleb S. O'Connor, MS • Brian M. Anderson, PhD • Bastien Rigaud, PhD • Bryan M. Fellman, MS • Kyle A. Jones, PhD • Kristy K. Brock, PhD • Bruno C. Odisio, MD**

From the Departments of Interventional Radiology (Y.M.L., I.P., B.C.O.), Imaging Physics (C.S.O., B.M.A., B.R., K.A.J., K.K.B.), and Biostatistics (B.M.F.), The University of Texas MD Anderson Cancer Center, 1515 Holcombe Blvd, Houston, TX 77030. Received June 7, 2022; revision requested August 15; revision received November 10; accepted November 18. **Address correspondence to** B.C.O. (email: *bcodisio@mdanderson.org*).

Research reported in this publication was supported in part by the National Institutes of Health–National Cancer Institute (R01CA235564, R01CA221971, P30CA016672) and the Helen Black Image Guided Fund and an Apache Corporation Grant via the Image Guided Cancer Therapy Research Program at The University of Texas MD Anderson Cancer Center. I.P. supported by a Postdoc.Mobility Fellowship from the Swiss National Science Foundation (P2BEP3_195444).

* K.K.B. and B.C.O. are co-senior authors.

Conflicts of interest are listed at the end of this article.

See also the editorial by Sofocleous in this issue.

Radiology 2023; 307(2):e221373 • https://doi.org/10.1148/radiol.221373 • Content codes: VA IR CT

Background: Confirming ablation completeness with sufficient ablative margin is critical for local tumor control following colorectal liver metastasis (CLM) ablation. An image-based confirmation method considering patient- and ablation-related biomechanical deformation is an unmet need.

Purpose: To evaluate a biomechanical deformable image registration (DIR) method for three-dimensional (3D) minimal ablative margin (MAM) quantification and the association with local disease progression following CT-guided CLM ablation.

Materials and Methods: This single-institution retrospective study included patients with CLM treated with CT-guided microwave or radiofrequency ablation from October 2015 to March 2020. A biomechanical DIR method with AI-based autosegmentation of liver, tumors, and ablation zones on CT images was applied for MAM quantification retrospectively. The per-tumor incidence of local disease progression was defined as residual tumor or local tumor progression. Factors associated with local disease progression were evaluated using the multivariable Fine-Gray subdistribution hazard model. Local disease progression sites were spatially localized with the tissue at risk for tumor progression (<5 mm) using a 3D ray-tracing method.

Results: Overall, 213 ablated CLMs (mean diameter, 1.4 cm) in 124 consecutive patients (mean age, 57 years ± 12 [SD]; 69 women) were evaluated, with a median follow-up interval of 25.8 months. In ablated CLMs, an MAM of 0 mm was depicted in 14.6% (31 of 213), from greater than 0 to less than 5 mm in 40.4% (86 of 213), and greater than or equal to 5 mm in 45.1% (96 of 213). The 2-year cumulative incidence of local disease progression was 72% for 0 mm and 12% for greater than 0 to less than 5 mm. No local disease progression was observed for an MAM greater than or equal to 5 mm. Among 117 tumors with an MAM less than 5 mm, 36 had local disease progression and 30 were spatially localized within the tissue at risk for tumor progression. On multivariable analysis, an MAM of 0 mm (subdistribution hazard ratio, 23.3; 95% CI: 10.8, 50.5; $P < .001$) was independently associated with local disease progression.

Conclusion: Biomechanical deformable image registration and autosegmentation on CT images enabled identification and spatial localization of colorectal liver metastases at risk for local disease progression following ablation, with a minimal ablative margin greater than or equal to 5 mm as the optimal end point.

Supplemental material is available for this article.

Percutaneous thermal ablation is a widely used minimally invasive curative-intent local therapy for select patients with colorectal liver metastasis (CLM) and is used as a stand-alone treatment or in combination with resection (1). Despite its several advantages, historically it has been mostly reserved for patients who are not eligible for surgery owing to relatively high rates of hepatic recurrence compared with surgery (2–4). Several patient-, tumor-, and ablation-related characteristics are associated with improved local tumor control after CLM ablation (5–10). Among those, complete tumor coverage with a sufficient ablation margin is considered one of the most critical factors for local tumor control (7,8,11). Presently, an ablation margin of greater than or equal to 5 mm, ideally greater than or equal to 10 mm, is considered optimal according to studies using two-dimensional anatomic landmarks–based margin visual assessment (6,7,12,13).

Recently, assessment of ablation margins by ablation confirmation software has been shown in small retrospective series to outperform visual assessment of ablation margins (14), provide volumetric assessment of ablation margins, and identify tumors at risk for local tumor progression (15–17). Three-dimensional (3D) ablation margin assessment requires dedicated imaging registration software to compare and integrate pre- and postprocedure images. Most of the current 3D methods rely on rigid image registration or intensity-based deformable registration. Both of these techniques are affected by registration errors related to liver deformity due to patient positioning and breathing, ablation

Abbreviations

AI = artificial intelligence, CLM = colorectal liver metastasis, DIR = deformable image registration, MAM = minimal ablative margin, SHR = subdistribution hazard ratio, 3D = three-dimensional

Summary

Ablative margin quantified using biomechanical deformable CT image registration with artificial intelligence–based autosegmentation was strongly associated and spatially localized within local disease progression after colorectal liver metastasis thermal ablation, and a minimal ablative margin greater than or equal to 5 mm was associated with optimal local tumor control.

Key Results

- In this retrospective study of 124 patients with 213 ablated colorectal liver metastases, when applying biomechanical deformable CT image registration with autosegmentation, no local disease progression was observed, with a minimal ablative margin (MAM) greater than or equal to 5 mm.
- At multivariable analysis, an MAM of 0 mm (subdistribution hazard ratio, 23.3; $P < .001$) was the dominant independent factor associated with local disease progression.
- Thirty of 36 sites (83%) of local disease progression were spatially localized within areas defined as tissue at risk for tumor progression (MAM <5 mm) using a three-dimensional ray-tracing method.

applicator placement, hydrodissection, ablation-related tissue attenuation and volumetric changes, contrast medium attenuation, and artifacts (15,18–20).

Currently, to our knowledge, there are no commercially available ablation confirmation methods that take into consideration the biomechanical properties of the liver and its deformation. We recently proposed and modified a biomechanical deformable image registration (DIR) method (21), which has been integrated into a radiation therapy treatment planning system to guide liver-directed therapies (22,23), to mitigate spatial uncertainties and increase precision and accuracy for minimal ablative margin (MAM) quantification after liver ablation (24).

The aim of this retrospective study was to evaluate a biomechanical DIR ablation confirmation method incorporating ablation-specific artificial intelligence (AI)–based autosegmentation for MAM quantification and the association with local disease progression in patients with CLMs undergoing CT-guided thermal ablation.

Materials and Methods

Patients

After approval by our institutional review board with a waiver of informed consent, a single-institution liver ablation registry (IRB no. PA-15–0566) was retrospectively surveyed to identify consecutive patients with CLMs who underwent liver ablation from October 2015 to March 2020 for this Health Insurance Portability and Accountability Act–compliant study. Patients were eligible forpercutaneous microwave ablation or radiofrequency ablation if they presented with up to five CLMs, each measuring less than or equal to 5 cm, and with no more than three extrahepatic sites of disease (including pulmonary nodules, lymph nodes, and peritoneal nodules). Selection criteria are described in Figure 1.

Ablation Procedure

All ablation procedures were performed with CT guidance by eight board-certified interventional radiologists with 6–13 years of experience, with patients under general anesthesia. All procedures were performed with curative intent, and the ablation end point was an ablative margin greater than or equal to 5 mm, which was evaluated by comparing pre- and postablation contrast-enhanced CT images using a two-dimensional, anatomic landmarks–based margin visual assessment method (25). Ablations were performed using microwave (NeuWave; Ethicon) as the first thermal ablation modality choice or radiofrequency (Cool-tip; Covidien) as an alternative. Patients were discharged home within 24 hours of the procedure if there were no complications. Ablation procedure details are provided in Appendix S1.

Ablation Outcomes Assessment and Definitions

Ablation outcomes were assessed according to reporting standards for ablation (26,27). Postablation contrast-enhanced CT, MRI, or PET examinations were used to assess imaging-related oncologic outcomes. All available cross-sectional images were evaluated independently by two interventional radiologists (B.C.O. and Y.M.L., with 13 and 5 years of experience, respectively), who were blinded to the results of MAM quantification according to the biomechanical DIR method, to determine the

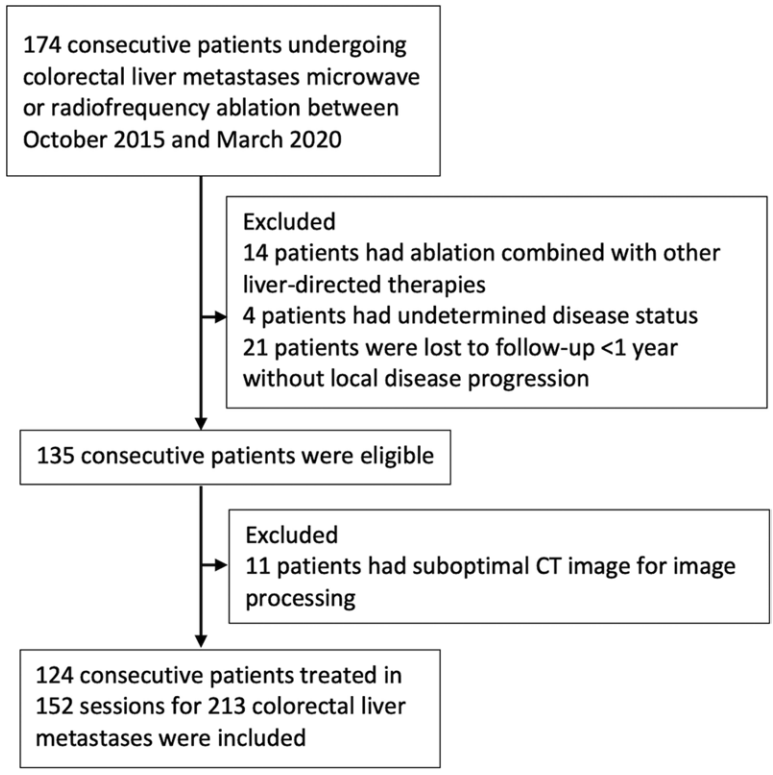

Figure 1: Flowchart shows patient inclusion and exclusion criteria.

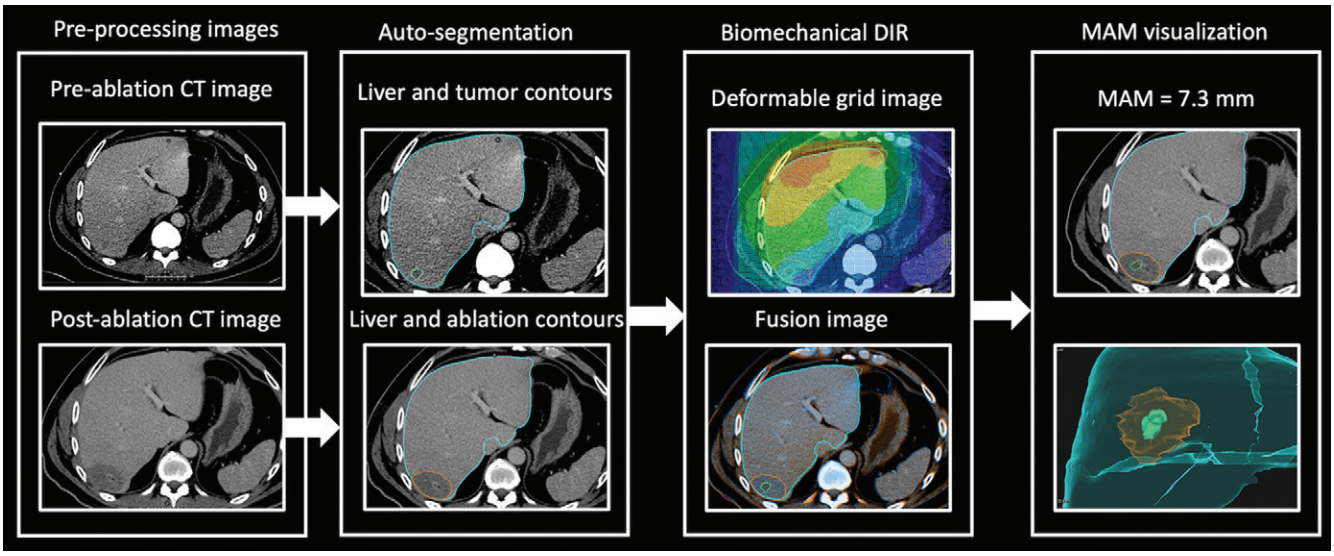

Figure 2: Flow diagram shows the steps in biomechanical deformable image registration (DIR) and minimal ablative margin (MAM) quantification in a 67-year-old man with solitary colorectal liver metastasis. Left: Pre- and postablation axial contrast-enhanced CT images with artificial intelligence–based autosegmentation show the liver, tumor, and ablation zone. Right: Biomechanical DIR is performed to register the pre- and postablation CT images. Then, the MAM is computed and visualized in images with two-dimensional and three-dimensional volume rendering.

oncologic outcomes of each ablated tumor. Disagreements on oncologic outcomes were resolved by consensus. Technique efficacy was defined as complete ablation of macroscopic tumor, as evidenced by initial follow-up imaging with no residual tumor. Residual tumor was defined as tumor foci within or at the edge of the ablation zone at initial follow-up imaging. Local tumor progression was defined as tumor foci within or at the edge of the ablation zone after at least one cross-sectional imaging study had demonstrated complete ablation. Local disease progression was defined as residual tumor or local tumor progression. Time to local disease progression was defined as the time between ablation and the first imaging evidence of residual tumor or local tumor progression. Perivascular tumors were defined on the baseline CT images as tumors located less than 10 mm from a vessel greater than or equal to 3 mm in diameter. Tumors were also classified as subcapsular (<10 mm from the liver edge) or nonsubcapsular. All definition assessments were made on a per-tumor basis for analysis of tumor-specific end points.

Biomechanical DIR and AI-based MAM Quantification

Pre- and postablation contrast-enhanced CT images (axial plane, portal venous phase, with an in-plane image resolution of 0.6–1.0 mm × 0.6–1.0 mm and an image thickness and interval of 2–5 mm) were uploaded to a radiation therapy treatment planning system (RayStation, version 9B; RaySearch Laboratories) for AI-based autosegmentation, biomechanical DIR, MAM quantification, and spatial localization (24). If available, intraprocedural preablation and final postablation contrast-enhanced CT images were used. For cases without intraprocedural preablation contrast-enhanced CT images for target tumor segmentation, the last diagnostic contrast-enhanced CT image before the procedure was used. For cases without intraprocedural postablation contrast-enhanced CT images for ablation zone segmentation, the initial follow-up contrast-enhanced CT image was used. Autosegmentation, biomechanical DIR, and MAM quantification were performed after ablation by a biomedical engineer (I.P., with 6 years of biomedical liver imaging experience) who was blinded to the oncologic outcomes. Spatial localization of local disease progression sites was performed by a biomedical engineer (C.S.O., with 2 years of biomedical liver imaging experience). All image processing was performed after the ablation procedure specifically for this study (Fig 2, Movie 1).

AI-based autosegmentation.—Two AI-based autosegmentation algorithms were integrated into the treatment planning system using the scripting engine and used to contour the liver, target tumor, and ablation zone (28,29). Manual correction was applied if needed.

Biomechanical DIR processing and visualization.—A biomechanical DIR method based on finite element modeling, which has been integrated and validated in the treatment planning system, was performed (22). Details are provided in Appendix S1.

Quantification of MAM.—The MAM was computed as the shortest distance between the segmented boundaries of the target tumor and the ablation zone on postablation contrast-enhanced CT images (Fig 3). The MAM was defined as a nonnegative number, with 0 mm indicating that the ablative margin and tumor contours overlapped (24). For subcapsular or perivascular tumors, calculation of the MAM did not include the area abutting the liver capsule or adjacent vessel. All the images could be assessed in two-dimensional and 3D volume rendering.

Spatial localization analysis between local disease progression and tissue at risk for tumor progression.—To spatially localize sites of local disease progression and insufficient MAM,

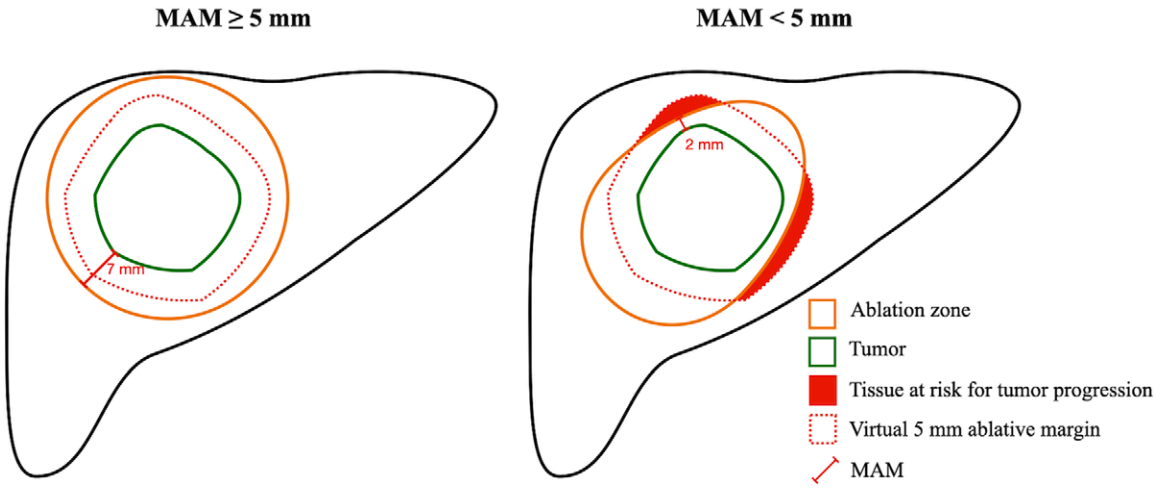

Figure 3: Schematic illustrations show minimal ablative margin (MAM) quantification. Left: The virtual 5-mm ablative margin (red dotted line) is completely covered by the ablation zone (orange solid line), with an MAM of 7 mm. Right: The virtual 5-mm ablative margin (red dotted line) is not completely covered by the ablation zone (orange solid line), with remaining tissue at risk for tumor progression (red) and an MAM of 2 mm.

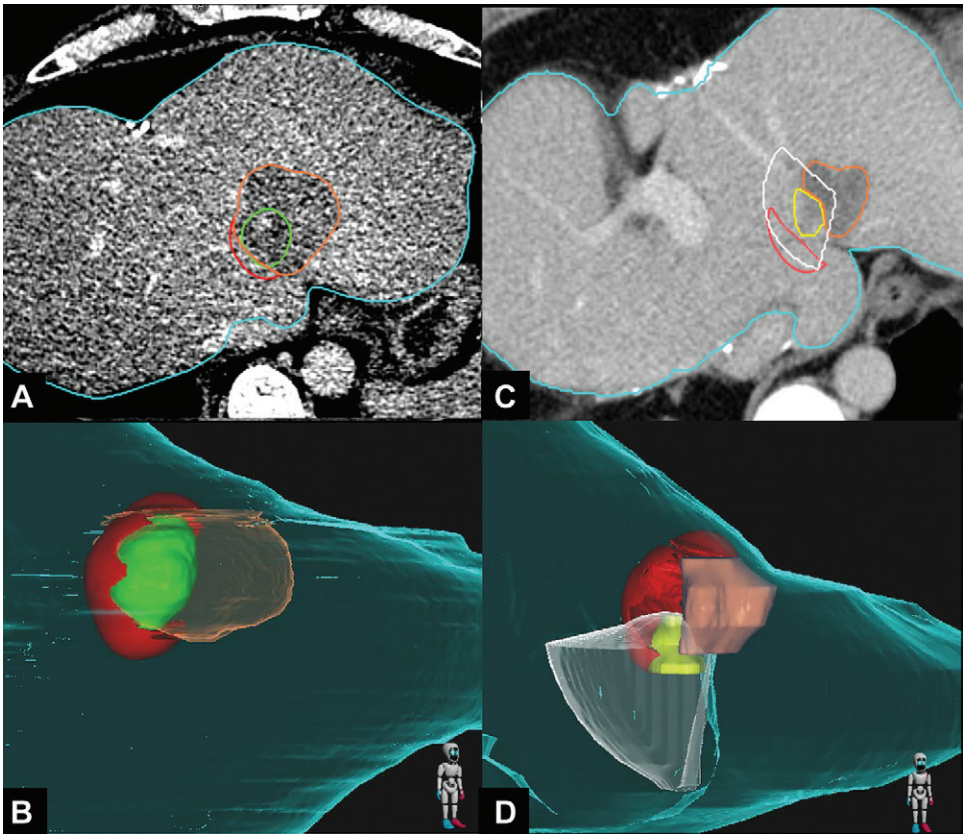

Figure 4: Images in a 41-year-old woman with colorectal liver metastasis who underwent CT-guided microwave ablation processed with the proposed biomechanical deformable image registration three-dimensional (3D) minimal ablative margin (MAM) quantification method. **(A, B)** Axial contrast-enhanced CT scan **(A)** obtained immediately after microwave ablation and corresponding 3D CT volume rendering **(B)** show autosegmentation of the tumor (green) and ablation zone (orange). Tissue at risk for tumor progression (red) is defined as the expanded tumor tissue not covered by the virtual 5-mm ablative margin. The MAM was determined to be 0 mm. **(C, D)** Axial contrast-enhanced CT scan **(C)** obtained 6 months after ablation and corresponding 3D CT volume rendering **(D)** show local tumor progression (yellow) and the corresponding radiating cone (white), which encompasses the tissue at risk for tumor progression (red), indicating that the site of local tumor progression is spatially correlated with the tissue at risk for tumor progression. The ablation zone (orange) has involuted compared with previous CT images.

a 3D ray-tracing method was used (24). Briefly, in tumors with an MAM less than 5 mm, a virtual 5 mm ablative margin was created on postablation contrast-enhanced CT images. In this region, the tissue not covered by ablation zone was defined as tissue at risk for tumor progression (Fig 3). The postablation contrast-enhanced CT image showing tissue at risk for tumor progression and the first CT image showing local disease progression were used. First, on the CT image showing local disease progression, a radiating cone was created originating from the center of the ablation zone covering the margins of local disease progression. Then, the first CT image showing local disease progression and the postablation contrast-enhanced CT image were rigidly registered with hepatic vasculature proximal to the ablation zone to account for temporal volume changes in the ablation zone. If the cone overlapped with tissue at risk for tumor progression, the site of local disease progression was considered to have occurred in the region of the tissue at risk for tumor progression (Fig 4, Movie 2).

Table 1: Patient Baseline Demographic and Clinical Characteristics

Characteristic	Value (n = 124)
Age (y)	57 ± 12
Sex	
M	55 (44)
F	69 (56)
Colorectal liver metastasis presentation	
Metachronous	57 (46)
Synchronous	67 (54)
Extrahepatic metastasis	
Yes	89 (72)
No	35 (28)
Disease-free interval (mo)*	
>12	26 (21)
≤12	98 (79)
Prior chemotherapy	
Yes	88 (71)
No	36 (29)
Carcinoembryonic antigen level (ng/mL)†	
<5	69 (68)
≥5	32 (32)
Neutrophil-to-lymphocyte ratio before ablation	
≤3	75 (60)
>3	49 (40)
RAS mutation status†	
Mutant	60 (49)
Wild-type	62 (51)
No. of procedures	152
No. of tumors ablated per procedure	
1	96 (63.2)
2	38 (25.0)
3	13 (8.6)
4	5 (3.3)

Note.—Data are mean ± SD and numbers of patients or procedures, with percentages in parentheses.

* From diagnosis of primary colorectal cancer to diagnosis of colorectal liver metastasis.

† Not all patients had available data; the carcinoembryonic antigen level was available in 101 patients and RAS mutation status was available in 122 patients.

Table 2: Tumor Characteristics

Characteristic	Value (n = 213)
Ablation modality	
Radiofrequency	13 (6.1)
Microwave	200 (93.9)
Intraprocedural contrast-enhanced CT*	
Yes	88 (41.3)
No	125 (58.7)
Time interval between last diagnostic CT and ablation (d)†	30 (20–41)
Time interval between initial follow-up CT and ablation (d)†	50 (36–69)
Tumor size (cm)	
Mean‡	1.4 ± 0.7 (range, 0.4–4)
<1	55 (25.8)
1–2	114 (53.5)
2–3	31 (14.6)
3–4	11 (5.2)
≥4	2 (0.9)
Tumor volume (mL)†	0.8 (0.3–1.6)
Tumor location, per liver segment	
Segment I	5 (2.3)
Segment II	20 (9.4)
Segment III	19 (8.9)
Segment IV	35 (16.4)
Segment V	20 (9.4)
Segment VI	31 (14.6)
Segment VII	35 (16.4)
Segment VIII	48 (22.5)
Tumor location	
Subcapsular	98 (46.0)
Nonsubcapsular	115 (54.0)
Proximity to vessel	
Perivascular	55 (25.8)
Nonperivascular	158 (74.2)
Minimal ablative margin (mm)	
0	31 (14.6)
>0 to <5	86 (40.4)
≥5§	96 (45.1)
Volume of tissue at risk for tumor progression (mL)†	0.04 (0–0.3)

Note.—Except where indicated, data are numbers of tumors, with percentages in parentheses. MAM = minimal ablative margin.

* Includes both pre- and postablation contrast-enhanced CT.

† Data are medians, with IQRs in parentheses.

‡ Data are mean ± SD, with the range in parentheses.

§ For statistical purposes, tumors with an MAM greater than or equal to 10 mm (n = 7, 3.3%) were included with MAM greater than or equal to 5 mm according to our predefined MAM categorization. Please refer to the Materials and Methods section for further details.

Statistical Analysis

The primary end point was to determine if the MAM is an independent predictor of local disease progression. The secondary end points were to spatially correlate the tissue at risk for tumor progression with sites of local disease progression and compare outcomes between CLMs with MAMs of 0 mm, greater than 0 to less than 5 mm, and greater than or equal to 5 mm. Based on the previous study (24), we assumed that an MAM greater than or equal to 10 mm would be a rare occurrence and, therefore, it was not categorized for statistical purposes. Patient-level data were summarized for the first ablation session, and tumor characteristics were summarized across all tumors. Each ablated CLM was considered an independent event. Differences in the volume of tissue at risk for tumor progression between different statuses of local disease progression were tested using the Mann-Whitney U test. The cumulative incidence function was used to estimate the time to local disease progression, with death without local disease progression considered a competing event. Associations

between time to local disease progression and clinical factors were assessed with univariable and multivariable competing-risks analyses with a Fine-Gray subdistribution hazard model (30). Finally, the percentage of tumors with local disease progression for which local disease progression was spatially localized within tissue at risk for tumor progression was determined. Categorical data are expressed as frequencies with percentages, and quantitative data are expressed as means ± SDs or medians with IQRs, as appropriate. The Shapiro-Wilk method was used for normality testing. $P < .05$ was considered to indicate a statistically significant difference. All statistical analyses were performed by a senior biostatistician (B.M.F., with 12 years of biostatistics experience) using Stata/MP (version 17.0; StataCorp).

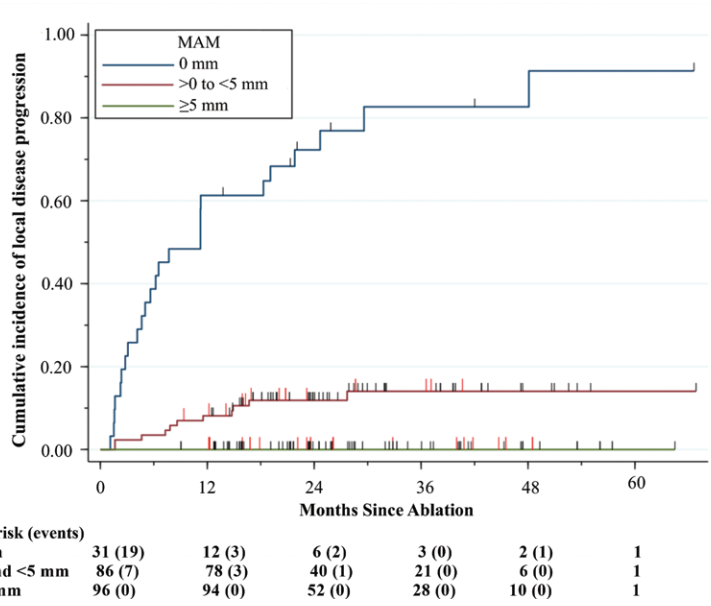

Figure 5: Cumulative incidence curve shows the per-tumor cumulative incidence of local disease progression over time stratified by the three-dimensional minimal ablative margin (MAM). Vertical red lines indicate death events and vertical black lines indicate censoring, with death as a competing risk.

Results

Patient Characteristics

The study included 124 consecutive patients (mean age, 57 years ± 12 [SD]; 69 women) with 213 CLMs treated in 152 sessions (median number of ablated CLMs per session, 1 [IQR, 1–2]) (Fig 1). Baseline patient and tumor characteristics are summarized in Table 1 and Table 2, respectively.

Ablation Outcomes

The ablation technique efficacy was 96.7% (206 of 213 CLMs). Over a median follow-up time of 25.8 months, residual tumor was noted in seven of 213 (3.3%) ablated tumors, and local tumor progression developed in 29 of 213 (13.6%) ablated tumors. The 1-year and 2-year cumulative incidences of local disease progression were 12% (95% CI: 8, 17) and 16% (95% CI: 11, 21), respectively. Interobserver variability for local disease progression assessment is detailed in Appendix S1.

Biomechanical DIR MAM Quantification

Of the 213 ablated tumors, 31 (14.6%) had an MAM of 0 mm, 86 (40.4%) had an MAM ranging from greater than 0 to less than 5 mm, and 96 (45.1%) had an MAM greater than or equal to 5 mm (Table 2). Local disease progression was noted in 80.6% (25 of 31) of the tumors with an MAM of 0 mm and 12.8% (11 of 86) of the tumors with an MAM ranging from greater than 0 to less than 5 mm. No local disease progression was documented among the tumors with an MAM greater than or equal to 5 mm. The 1-year and 2-year cumulative incidences of local disease progression were 61% (95% CI: 42, 76) and 72% (95% CI: 52, 85), respectively, among the tumors with an MAM of 0 mm, and 8% (95% CI: 4, 15) and 12% (95% CI: 6, 20), respectively, among the tumors with an MAM ranging from greater than 0 to less than 5 mm. Local disease progression for tumors with an MAM greater than or equal to 5 mm was not observed (Fig 5).

Among the 117 tumors with an MAM less than 5 mm, 36 (30.8%) had local disease progression. The median volume of tissue at risk for tumor progression was 0.2 mL (IQR, 0.1–0.3 mL) in tumors without local disease progression and 1.4 mL (IQR, 0.6–2.9 mL) in tumors with local disease progression ($P < .001$). Among the 117 tumors with an MAM less than 5 mm, a volume of tissue at risk for tumor progression less than 1 mL was noted in 90.1% (73 of 81) of the tumors without local disease progression and in 38.9% (14 of 36) of the tumors with local disease progression ($P < .001$).

The effect of RAS mutation status, CT section thickness, and tumor size on the MAM are detailed in Appendix S1.

Univariable Competing-Risks Regression Analysis for Local Disease Progression

Univariable competing-risks regression analysis showed that a serum carcinoembryonic antigen level greater than or equal to 5 ng/mL (subdistribution hazard ratio [SHR], 2.5; 95% CI: 1.2, 5.1; $P = .02$), tumor size greater than or equal to 2 cm (SHR, 2.9; 95% CI: 1.5, 5.8; $P = .002$), tumor volume (SHR, 1.1; 95% CI: 1.0, 1.2; $P = .02$), MAM of 0 mm (SHR, 25.0; 95% CI: 12.5, 50.0; $P < .001$), and volume of tissue at risk for tumor progression (SHR, 1.3; 95% CI: 1.2, 1.4; $P < .001$) were risk factors affecting the time to local disease progression (Table 3).

Multivariable Competing-Risks Regression Analysis for Local Disease Progression

Multivariable competing-risks regression analysis showed that tumor size greater than or equal to 2 cm (SHR, 2.8; 95% CI: 1.4, 5.5; $P = .002$) and an MAM of 0 mm (SHR, 23.3; 95% CI: 10.8, 50.5; $P < .001$) were independently associated with local disease progression after thermal ablation (Fig 6).

Spatial Localization between Sites of Local Disease Progression and Tissue at Risk for Tumor Progression

According to the 3D ray-tracing method, 83% (30 of 36) of the tumors with local disease progression had the disease progression site spatially correlated with tissue at risk for tumor progression. Among the tumors with local disease progression spatially correlated with tissue at risk for tumor progression, the median MAM was 0 mm (IQR, 0–0 mm) and the median volume of tissue at risk for tumor progression was 1.5 mL (IQR, 0.7–4.1 mL).

Discussion

Accurate and reproducible methods to evaluate ablation completeness have the potential to improve local tumor control rates in patients undergoing ablation of colorectal liver metastases (CLMs). In this study, using biomechanical deformable image registration with AI-based autosegmentation for minimal ablative margin (MAM) quantification, we found that an MAM greater than or equal to 5 mm was achieved in only 45% of ablated tumors, even though all procedures were performed with an ablation end point of a margin greater than or equal to 5 mm according to visual inspection. Furthermore, an MAM of 0 mm was a significant independent predictor of local disease progression (subdistribution hazard ratio, 23.3; $P < .001$) and no local disease progression was observed in CLMs with an MAM greater than or equal to 5 mm.

Accurate and precise image registration is critical in MAM quantification. Previous studies excluded tumors that were not visible on intraprocedural CT images because of the intrinsic challenges of performing image registration with diagnostic images obtained days or weeks before the procedure (15,17). Also, intraprocedural image registration can be difficult because of tissue deformation related to breathing, hydrodissection, applicator placement, or ablation-related tissue changes. Although two-dimensional visual inspection comparing pre- and postablation contrast-enhanced CT images side by side using anatomic landmarks is a simple and direct method, it is time-consuming, prone to operator bias, does not consider biomechanical changes of liver tissue related to ablation, and is less accurate than a 3D method (25,31). The proposed biomechanical DIR method has been validated in liver radiation therapy, which is notorious for resulting in remarkable temporal liver deformation (23). In our study, the biomechanical DIR method was effective in cases with nonintraprocedural contrast-enhanced CT images, while also accounting for the biomechanical changes related to the ablation procedure.

Although our study showed a strong association between an MAM of less than 5 mm and local disease progression, 69% (81 of 117) of the CLMs with an MAM less than 5 mm had no local disease progression and most of them had a volume of tissue at risk for tumor progression of less than 1 mL. Previous studies using visual inspection or ablation confirmation software for MAM quantification with different thresholds have shown high false-positive rates as well (7,16,17,32). The high false-positive rate in our study may be due to the intrinsic margin of error of the proposed DIR method (2.8 mm) (22) and the nonstandardized CT protocol, which was reflected in a volume of tissue at risk for tumor progression of less than 1 mL.

Table 3: Univariable Analysis of Factors Associated with Local Disease Progression Using the Competing-Risks Regression Model

Variable	SHR	*P* Value
Age (y)	0.99 (0.9, 1.1)	.76
Colorectal liver metastasis presentation		.36
Metachronous	Reference	
Synchronous	1.4 (0.7, 2.7)	
Extrahepatic metastasis		.33
No	Reference	
Yes	1.5 (0.7, 3.3)	
Disease-free interval ≤12 months*		.10
No	Reference	
Yes	0.6 (0.3, 1.1)	
Neoadjuvant chemotherapy		.65
No	Reference	
Yes	0.9 (0.4, 1.7)	
Carcinoembryonic antigen level (ng/mL)		.02
<5	Reference	
≥5	2.5 (1.2, 5.1)	
Neutrophil-to-lymphocyte ratio before ablation		.09
≤3	Reference	
>3	1.1 (0.9, 1.3)	
RAS mutation status		.94
Wild-type	Reference	
Mutant	1.0 (0.5, 2.0)	
Intraprocedural contrast-enhanced CT†		.09
No	Reference	
Yes	0.5 (0.3, 1,1)	
Tumor size (cm)		.002
<2	Reference	
≥2	2.9 (1.5, 5.8)	
Tumor volume (mL)	1.1 (1.0, 1.2)	.02
Tumor location		.15
Nonsubcapsular	Reference	
Subcapsular	1.6 (0.8, 3.1)	
Proximity to vessel		.62
Nonperivascular	Reference	
Perivascular	1.2 (0.9, 2,5)	
Minimal ablative margin (mm) (continuous)	0.4 (0.3, 0.5)	<.001
Minimal ablative margin (mm)		<.001
>0	Reference	
0	25.0 (12.5, 50.0)	
Volume of tissue at risk for tumor progression (mL)	1.3 (1.2, 1.4)	<.001

Note.—Data in parentheses are 95% CIs. SHR = subdistribution hazard ratio.

* From diagnosis of primary colorectal cancer to diagnosis of liver metastasis.

† Includes both pre- and postablation contrast-enhanced CT.

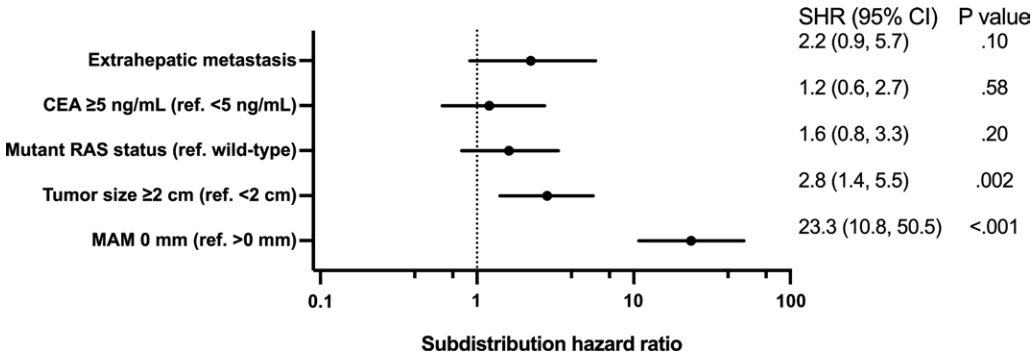

Figure 6: Forest plot based on multivariable analysis of factors associated with local disease progression using the competing-risks regression model shows that tumor size greater than or equal to 2 cm and a minimal ablative margin (MAM) of 0 mm are independently associated with local disease progression after thermal ablation. CEA = carcinoembryonic antigen, ref = reference, SHR = subdistribution hazard ratio.

To overcome such limitations, standardized intraprocedural contrast-enhanced CT protocols and reproducible methods for MAM quantification are urgent.

Several studies have tried to define the optimal MAM for complete tumor control after CLM ablation. In studies using conventional visual margin assessment comparing pre- and postablation two-dimensional CT images, higher local tumor progression rates were reported with margins greater than 5 mm compared with margins greater than 10 mm. Therefore, a margin greater than 10 mm was recommended as optimal local tumor control (7,8,12). However, studies using both rigid and nonrigid imaging registration and 3D margin assessment showed that a margin greater than 2–3 mm was associated with no local tumor progression (15,17). In the present study, we found no local disease progression among CLMs with an MAM greater than or equal to 5 mm. This may indicate that achieving margins greater than 10 mm, which is intrinsically challenging because of the need to ablate a larger volume of tissue, might not be required if the biomechanical DIR method for MAM quantification is applied. Our results suggest that an MAM greater than or equal to 5 mm might be the optimal end point for CLM ablation. Therefore, the definition of the optimal ablation margins should be dependent on the specific ablation confirmation method used. The use of a dedicated ablation confirmation software during ablation procedures might improve the ability to achieve optimal ablation margins, and the proposed method provides a potential solution. Our ongoing phase II randomized trial (ClinicalTrials.gov registration no. NCT04083378) is evaluating the role of our method, with the primary end point of achieving an MAM greater than or equal to 5 mm, as an intraprocedural ablation confirmation tool (33).

An interesting finding in our study was that, contrary to prior studies, RAS mutation status was not demonstrated to be an independent factor for local disease progression ($P = .20$) (6,13,34). There are several potential reasons for this lack of association. First, some of the prior studies expanded the definition of local tumor progression by including the appearance of tumor foci within 1 cm of the edge of the ablation zone (6,13), which was different from our study. Second, it is conceivable that the patients included in our study have been treated with larger ablation zones given the current understanding that larger ablative margins are needed for patients with CLM, especially those with RAS mutation. This could have offset the effects of RAS mutation status on local tumor outcomes. Prior studies correlating ablation margins and RAS mutation status had ablation margins evaluated by visual inspection instead of software-based quantitative MAM analysis, which might have overestimated the MAM and, therefore, precludes accurate comparison with our present series. Finally, the lack of association between RAS mutation and local tumor outcomes is in keeping with a recent study assessing the MAM using a rigid registration method, which demonstrated that *KRAS* mutation was not a predictor of ablation site recurrence on multivariable analysis after the MAM was taken into account (15).

Our study had several limitations. First, a small number of local disease progression events ($n = 36$) were observed, which may have biases in regression coefficients and predictive accuracy at multivariable analysis. However, the sample size in our study was larger than in other studies related to MAM assessment of CLM ablation. Second, the retrospective design precluded ruling out selection bias. Third, variations in CT timing and acquisition parameters may have limited the accuracy of MAM quantification. Fourth, we did not compare the MAM quantified by the proposed method with that of other software or visual inspection, which warrants further study. Finally, the competing-risks regression analysis was a patient-clustered tumor-based analysis and did not take into account within-patient correlation given the limitation of this method.

In conclusion, the proposed biomechanical deformable image registration three-dimensional minimal ablative margin (MAM) quantification method with autosegmentation on CT images showed a strong association between the MAM and local disease progression. No local disease progression occurred for colorectal liver metastases (CLMs) with an MAM greater than or equal to 5 mm, which was achieved in less than 50% of the ablated CLMs. Sites of local disease progression were localized in more than 80% of the cases within areas with an MAM less than 5 mm. An ongoing phase II clinical trial with a standardized intraprocedural contrast-enhanced CT imaging protocol is currently evaluating the role of this method for intraprocedural feedback and its potential clinical benefit (33).

Acknowledgment: We thank Stephanie Deming, Research Medical Library, MD Anderson Cancer Center, for editing the article.

Author contributions: Guarantors of integrity of entire study, **B.M.F., B.C.O.**; study concepts/study design or data acquisition or data analysis/interpretation, all authors; manuscript drafting or manuscript revision for important intellectual content, all authors; approval of final version of submitted manuscript, all authors; agrees to ensure any questions related to the work are appropriately resolved, all authors; literature research, **Y.M.L., I.P., B.M.A., B.C.O.**; clinical studies, **Y.M.L., I.P., C.S.O., B.R., K.A.J., B.C.O.**; experimental studies, **B.M.A., B.R., K.K.B.**; statistical analysis, **B.R., B.M.F.**; and manuscript editing, **Y.M.L., I.P., B.M.A., B.M.F., K.A.J., K.K.B., B.C.O.**

Disclosures of conflicts of interest: Y.M.L. No relevant relationships. **I.P.** No relevant relationships. **C.S.O.** No relevant relationships. **B.M.A.** No relevant relationships. **B.R.** No relevant relationships. **B.M.F.** No relevant relationships. **K.A.J.** No relevant relationships. **K.K.B.** Grants from the National Institutes of Health and RaySearch Laboratories; licensing agreement with RaySearch Laboratories; travel support from The American Association of Physicists in Medicine; patents planned, issued, or pending; advisory board, RaySearch Laboratories. **B.C.O.** Research grants from Siemens Healthineers and Johnson & Johnson; consulting fees from Siemens Healthineers.

References

1. National Comprehensive Cancer Network. Colon Cancer (Version 1.2022). https://www.nccn.org/professionals/physician_gls/pdf/colon.pdf. Accessed August 17, 2022.
2. Otto G, Düber C, Hoppe-Lotichius M, König J, Heise M, Pitton MB. Radiofrequency ablation as first-line treatment in patients with early colorectal liver metastases amenable to surgery. Ann Surg 2010;251(5):796–803.
3. Abdalla EK, Vauthey JN, Ellis LM, et al. Recurrence and outcomes following hepatic resection, radiofrequency ablation, and combined resection/ablation for colorectal liver metastases. Ann Surg 2004;239(6):818–825; discussion 825–827.
4. Mulier S, Ni Y, Jamart J, Michel L, Marchal G, Ruers T. Radiofrequency ablation versus resection for resectable colorectal liver metastases: time for a randomized trial? Ann Surg Oncol 2008;15(1):144–157.
5. Lin YM, Paolucci I, Brock KK, Odisio BC. Image-Guided Ablation for Colorectal Liver Metastasis: Principles, Current Evidence, and the Path Forward. Cancers (Basel) 2021;13(16):3926.
6. Calandri M, Yamashita S, Gazzera C, et al. Ablation of colorectal liver metastasis: Interaction of ablation margins and RAS mutation profiling on local tumour progression-free survival. Eur Radiol 2018;28(7):2727–2734.
7. Shady W, Petre EN, Gonen M, et al. Percutaneous Radiofrequency Ablation of Colorectal Cancer Liver Metastases: Factors Affecting Outcomes--A 10-year Experience at a Single Center. Radiology 2016;278(2):601–611.
8. Han K, Kim JH, Yang SG, et al. A Single-Center Retrospective Analysis of Periprocedural Variables Affecting Local Tumor Progression after Radiofrequency Ablation of Colorectal Cancer Liver Metastases. Radiology 2021;298(1):212–218.
9. Groeschl RT, Pilgrim CH, Hanna EM, et al. Microwave ablation for hepatic malignancies: a multiinstitutional analysis. Ann Surg 2014;259(6):1195–1200.
10. Odisio BC, Yamashita S, Huang SY, et al. Impact of Prior Hepatectomy History on Local Tumor Progression after Percutaneous Ablation of Colorectal Liver Metastases. J Vasc Interv Radiol 2018;29(3):395–403.e1.
11. Solbiati L, Ahmed M, Cova L, Ierace T, Brioschi M, Goldberg SN. Small liver colorectal metastases treated with percutaneous radiofrequency ablation: local response rate and long-term survival with up to 10-year follow-up. Radiology 2012;265(3):958–968.
12. Shady W, Petre EN, Do KG, et al. Percutaneous Microwave versus Radiofrequency Ablation of Colorectal Liver Metastases: Ablation with Clear Margins (A0) Provides the Best Local Tumor Control. J Vasc Interv Radiol 2018;29(2):268–275.e1.
13. Shady W, Petre EN, Vakiani E, et al. Kras mutation is a marker of worse oncologic outcomes after percutaneous radiofrequency ablation of colorectal liver metastases. Oncotarget 2017;8(39):66117–66127.
14. Laimer G, Schullian P, Putzer D, Eberle G, Goldberg SN, Bale R. Can accurate evaluation of the treatment success after radiofrequency ablation of liver tumors be achieved by visual inspection alone? Results of a blinded assessment with 38 interventional oncologists. Int J Hyperthermia 2020;37(1):1362–1367.
15. Ruiter SJS, Tinguely P, Paolucci I, et al. 3D Quantitative Ablation Margins for Prediction of Ablation Site Recurrence After Stereotactic Image-Guided Microwave Ablation of Colorectal Liver Metastases: A Multicenter Study. Front Oncol 2021;11:757167.
16. Kaye EA, Cornelis FH, Petre EN, et al. Volumetric 3D assessment of ablation zones after thermal ablation of colorectal liver metastases to improve prediction of local tumor progression. Eur Radiol 2019;29(5):2698–2705.
17. Laimer G, Jaschke N, Schullian P, et al. Volumetric assessment of the periablational safety margin after thermal ablation of colorectal liver metastases. Eur Radiol 2021;31(9):6489–6499. [Published correction appears in Eur Radiol 2022;32(1):737.]
18. Kim YS, Rhim H, Lim HK, Choi D, Lee MW, Park MJ. Coagulation necrosis induced by radiofrequency ablation in the liver: histopathologic and radiologic review of usual to extremely rare changes. RadioGraphics 2011;31(2):377–390.
19. Brace CL, Diaz TA, Hinshaw JL, Lee FT Jr. Tissue contraction caused by radiofrequency and microwave ablation: a laboratory study in liver and lung. J Vasc Interv Radiol 2010;21(8):1280–1286.
20. Galmén K, Freedman J, Toporek G, Goździk W, Harbut P. Clinical application of high frequency jet ventilation in stereotactic liver ablations - a methodological study. F1000 Res 2018;7:773.
21. Brock KK, Sharpe MB, Dawson LA, Kim SM, Jaffray DA. Accuracy of finite element model-based multi-organ deformable image registration. Med Phys 2005;32(6):1647–1659.
22. Velec M, Moseley JL, Svensson S, Hårdemark B, Jaffray DA, Brock KK. Validation of biomechanical deformable image registration in the abdomen, thorax, and pelvis in a commercial radiotherapy treatment planning system. Med Phys 2017;44(7):3407–3417.
23. Polan DF, Feng M, Lawrence TS, Ten Haken RK, Brock KK. Implementing Radiation Dose-Volume Liver Response in Biomechanical Deformable Image Registration. Int J Radiat Oncol Biol Phys 2017;99(4):1004–1012.
24. Anderson BM, Lin YM, Lin EY, et al. A novel use of biomechanical model-based deformable image registration (DIR) for assessing colorectal liver metastases ablation outcomes. Med Phys 2021;48(10):6226–6236.
25. Wang X, Sofocleous CT, Erinjeri JP, et al. Margin size is an independent predictor of local tumor progression after ablation of colon cancer liver metastases. Cardiovasc Intervent Radiol 2013;36(1):166–175.
26. Puijk RS, Ahmed M, Adam A, et al. Consensus Guidelines for the Definition of Time-to-Event End Points in Image-guided Tumor Ablation: Results of the SIO and DATECAN Initiative. Radiology 2021;301(3):533–540.
27. Ahmed M, Solbiati L, Brace CL, et al; Standard of Practice Committee of the Cardiovascular and Interventional Radiological Society of Europe. Image-guided tumor ablation: standardization of terminology and reporting criteria--a 10-year update. Radiology 2014;273(1):241–260.
28. Anderson BM, Rigaud B, Lin YM, et al. Automated segmentation of colorectal liver metastasis and liver ablation on contrast-enhanced CT images. Front Oncol 2022;12:886517.
29. Anderson BM, Lin EY, Cardenas CE, et al. Automated Contouring of Contrast and Noncontrast Computed Tomography Liver Images With Fully Convolutional Networks. Adv Radiat Oncol 2020;6(1):100464.
30. Fine JP, Gray RJ. A Proportional Hazards Model for the Subdistribution of a Competing Risk. J Am Stat Assoc 1999;94(446):496–509.
31. Vasiniotis Kamarinos N, Gonen M, Sotirchos V, et al. 3D margin assessment predicts local tumor progression after ablation of colorectal cancer liver metastases. Int J Hyperthermia 2022;39(1):880–887.
32. Vasiniotis Kamarinos N, Vakiani E, Gonen M, et al. Biopsy and Margins Optimize Outcomes after Thermal Ablation of Colorectal Liver Metastases. Cancers (Basel) 2022;14(3):693.
33. Lin YM, Paolucci I, Anderson BM, et al. Study Protocol COVER-ALL: Clinical Impact of a Volumetric Image Method for Confirming Tumour Coverage with Ablation on Patients with Malignant Liver Lesions. Cardiovasc Intervent Radiol 2022;45(12):1860–1867.
34. Dijkstra M, Nieuwenhuizen S, Puijk RS, et al. Primary Tumor Sidedness, RAS and BRAF Mutations and MSI Status as Prognostic Factors in Patients with Colorectal Liver Metastases Treated with Surgery and Thermal Ablation: Results from the Amsterdam Colorectal Liver Met Registry (AmCORE). Biomedicines 2021;9(8):962.